JOURNAL OF CATALYSIS 76, 188–207 (1982)

Multicomponent Catalysts for the Oxidation of Propylene to Acrolein: $Fe_2(MoO_4)_3$ Doped with Bi or Te

P. FORZATTI[1] AND P. L. VILLA

Istituto di Chimica Industriale "G. Natta" del Politecnico, Piazza Leonardo da Vinci 32, 20133 Milan, Italy

N. FERLAZZO

Euteco Impianti, Via Reali 4, 20037 Paderno Dugnano, Italy

AND

D. JONES

Istituto dei composti del carbonio contenenti eteroatomi e loro applicazioni, Consiglio Nazionale delle Ricerche, 40064 Ozzano Emilia (Bologna), Italy

Received October 28, 1981; revised February 19, 1982

Multicomponent molybdate catalysts consisting of $Fe_2(MoO_4)_3$ with different amounts of Bi or Te were used for the oxidation of propylene to acrolein and characterized by means of DT, TG, and DSC analyses, surface area measurements, X-ray diffraction, and ir, Raman, diffuse reflectance, and X-ray photoelectron spectroscopies. The effects of Bi and Te levels were investigated over a wide concentration range from 0.000064 to 0.256 g atoms of Bi or Te per mole of $Fe_2(MoO_4)_3$. Experimental evidence showed that: (i) Bi, Te, and Mo can enter the $Fe_2(MoO_4)_3$ structure in the interstitial sites; (ii) at low concentrations Bi and Te tend to concentrate at the catalyst surface; (iii) dopants on the catalyst surface show oxidation states above III for Bi and above IV for Te; (iv) the localization of Bi, Te, and Mo in the interstitial sites, together with the stabilization of the higher oxidation states of Bi and Te, prevents catalyst deactivation; (v) $Bi_3(FeO_4)(MoO_4)_2$ and MoO_3 are formed in the catalysts with high amounts of Bi and Te, respectively. The catalytic and analytical data lead to the following conclusions: (1) *selectivity* is related to surface properties such as the presence of surface Bi–O–M–O–Bi (or Bi–O–Bi) and Te–O–M–O–Te (or Te–O–Te) chain bonds and controlled valence conductivity involving two-electron transfer processes; (2) *activity* is related to bulk properties such as oxygen mobility and bulk conductivity that can change with the presence of Bi, Te, or Mo in the $Fe_2(MoO_4)_3$ interstitial sites; (3) the formation of $Bi_3(FeO_4)(MoO_4)_2$ and MoO_3 is not directly responsible for the catalytic properties observed.

INTRODUCTION

In recent years multicomponent molybdate (MCM) catalysts have come into use for the industrial oxidation and ammoxidation of propylene. Typical catalyst formulations are (*1–3*):

$$Mo_aFe_bBi_cMe_d^{2+}K_eP_fO_x, \qquad Me^{2+} = Ni, Co,$$

or alternatively (*4*):

$$Mo_aCe_bTe_cMe_d^{2+}O_x, \qquad Me^{2+} = Ni.$$

The catalysts are supported on silica when the reaction is performed in a fluidized bed. The patent information implies that there is always a molybdate system consisting of $Fe_2(MoO_4)_3$ or $Ce_2(MoO_4)_3$ combined with $Me^{2+}MoO_4$ and ill-defined bismuth or tellurium compounds.

Most of the studies reported in the literature focus on simple unsupported binary or ternary oxides, which should be similar in their catalytic character to more complex and supported oxides. Sleight and co-workers (*5–7*) studied defect molybdates and tungstates with scheelite structures having

[1] To whom correspondence should be addressed.

0021-9517/82/070188-20$02.00/0

the ideal formulas $Me^{2+}_{1-3x}Bi_{2x}{}^{3+}\phi_x MO_4$ and $Me^{1+}_{0.5-3x}Li^{3+}_{0.5+x}\phi_{2x}MO_4$ and came to the conclusion that the presence of both point defects and bismuth is essential for optimum catalytic performance. Villa *et al.* (*8*) investigated the bismuth-impregnated $Fe_2(MoO_4)_3$ system and proposed that the active and selective phase of the resulting Bi FeMo catalyst is Fe(III) molybdate with bismuth as dopant in interstitial or substitutional sites, probably as Bi^{5+}. An explanation along similar lines was given by Andrushkevich *et al.* (*9*) and by Forzatti *et al.* (*10, 11*) in order to account for the effect of the addition of tellurium to MoO_3 and to a large series of divalent and trivalent metal molybdates. These authors relate good catalytic performances in olefin oxidation to the occurrence of solid solutions with tellurium entering the lattice interstitially or substituting Mo^{6+}.

Other authors preferred a correlation between catalytic properties and the presence of a well-defined active and selective phase, given the fact that many compounds such as bismuth molybdates (*12*), Te_2MoO_7 (*13*), $Bi_3(FeO_4)(MoO_4)_2$ (*14*), and $MeTeMoO_6$, where Me is Cd, Co, Mg, Mn, and Zn (*15–17*), are active and selective catalysts for propylene oxidation and ammoxidation. However, all these compounds contain either Bi or Te and could, therefore, be self-doped by these elements, in a way similar to that outlined above.

More complex MCM catalysts of composition $Me_8{}^{2+}Me_3{}^{3+}BiMo_{12}$, where Me^{2+} is Ni, Co, Mn, and Mg and Me^{3+} is Fe, Cr, and Al, were investigated by Wolf and Batist (*18*) and Matsuura and Wolf (*19*). The results were interpreted in terms of an inner core of divalent metal molybdates with two surface shells: one directly at the surface, consisting of bismuth molybdates, and one below that, consisting of iron molybdate, the amount of iron increasing on going toward the core of the catalysts. This model was recently refined by Matsuura (*20*). However, an investigation by Prasada Rao and Menon (*21*) on a 50% $Ni_3Co_5Fe_3BiMo_{12}K_{0.1}PO_x$–50% SiO_2 catalyst tends to cast doubt on the BiMo skin concept. XPS measurements revealed the presence of Co, Fe, Mo, Ni, Bi, Si, and O on the surface of both fresh and used catalysts while the relative composition differed markedly depending on whether the catalyst had been exposed or not to ammoxidation conditions. Bertolini *et al.* (*22*), during a structural investigation of MCM catalysts containing Mo, Fe, Co, Ni, Bi, P, Si, K, and O, prepared a reproducible catalyst having high activity and selectivity and containing only two phases: $Fe_2(MoO_4)_3$ and β-$CoMoO_4$ in an appropriate ratio. Their catalyst was obtained by an accurate selection of preparation parameters and did not contain any bismuth molybdate phase.

In conclusion the scientific literature offers conflicting explanations of the performance of MCM catalysts. The catalytic behavior is related either to the presence of well-defined active and selective phases or to the doping action of bismuth and tellurium. However, this promoting–moderating effect has not yet been clarified. On the other hand, conclusive evidence has been provided to show that the presence of bismuth and tellurium is essential for good catalytic performance.

With this in mind our present investigation was performed along the following lines:

(i) Considering that $Fe_2(MoO_4)_3$ is a common constituent of commercial MCM catalysts and cannot be self-doped by Bi and Te, catalysts consisting of $Fe_2(MoO_4)_3$ and of Bi or Te added in small quantities were considered.

(ii) Such a comparative study was expected to clarify analogies as well as differences in the action of Bi and Te.

(iii) To assure catalyst homogeneity the catalysts were prepared by spray drying.

(iv) The catalysts were characterized by DT, TG, and DSC analyses, X-ray diffraction, and ir, Raman, diffuse reflectance, and X-ray photoelectron spectroscopies, giving a wide range of information on the Fe_2

$(MoO_4)_3$ phase, other spurious phases, Bi and Te dopants, and the nature of the catalyst surface.

(v) The effect of Bi and Te additions was investigated over a large concentration range, from very low levels up to those used in commercial MCM catalysts. This was done with the aim of clarifying in which concentration range the changes in activity and selectivity take place and whether these changes can be related to surface composition, bulk composition, or to any other properties of the catalyst.

METHODS

Preparation of Catalysts

$Fe_2(MoO_4)_3$ was obtained by dissolving 52.97 g of $(NH_4)_6Mo_7O_{24} \cdot 4H_2O$ in 350 ml of water at 80°C. Melted $Fe(NO_3)_3 \cdot 9H_2O$, 80.8 g, was added to the solution and the resulting slurry diluted to 600 ml over 30 min. The pH was raised to 5 by repeated NH_4OH additions during aging at 80°C for 4 hr. The slurry was finally spray dried and gradually heated to 510°C over 6 hr and then kept at this temperature for 5 hr more. There were two different preparations of $Fe_2(MoO_4)_3$, cited as FeMo-O(I) and FeMo-O(II).

$Fe_2(MoO_4)_3$ catalysts doped with Bi were prepared in the same way with the desired amount of $Bi(NO_3)_3 \cdot 5H_2O$ being melted together with the $Fe(NO_3)_3 \cdot 9H_2O$. $Fe_2(MoO_4)_3$ catalysts doped with Te were prepared by adding H_6TeO_6 to the $(NH_4)_6Mo_7O_{24} \cdot 4H_2O$ solution. In both cases molybdenum was completely salified with iron. The catalysts were labeled according to their Bi or Te loading: e.g., FeMoBi-0.064 indicates a sample in which 1 mole of $Fe_2(MoO_4)_3$ is doped with 0.064 g atoms of Bi.

$Bi_3(FeO_4)(MoO_4)_2$ was prepared according to Ref. (*23*).

Characterization of Catalysts

X-Ray powder patterns were recorded using a Philips PW 1140/90 counter diffractometer with Fe $K\alpha$–Mn filtered radiation.

Infrared spectra were obtained using KBr disks on a Perkin–Elmer 457 infrared spectrometer.

Raman spectra were measured on a Cary 83 laser Raman spectrophotometer (4880-Å excitation).

Diffuse reflectance spectra were recorded with a Cary 15 instrument provided with a diffuse reflectance attachment against a bulk of $BaSO_4$.

DTA and TG experiments were performed with a Mettler Analyser T2-WR with a 5°C/min heating rate.

DSC measurements were recorded on a DSC 2 Perkin–Elmer instrument with a 20°C/min heating rate.

Surface areas were determined with a BET dynamic system.

The X-ray photoelectron spectra were obtained with an AEI ES200B photoelectron spectrometer using an Al $K\alpha$ source. The samples were mounted on double-sided adhesive tape in powder or pellet form and cooled during analysis to prevent charring of the adhesive backing. Peak positions were measured (±0.2 eV) relative to each other and to the C_{1s} contamination peak. Relative signal intensities of the elements present were obtained by cutting out and weighing the area under each of the corresponding peaks (Fe_{2p}, Mo_{3d}, Bi_{4f}, Te_{3d}, Fe_{3p}, Mo_{4p}). This method gave relative signal intensity values with a reproducibility of ±5%.

Activity Measurements

The oxidation of C_3H_6 was performed in an AISI 316 stainless-steel fixed-bed reactor (i.d. 5.4 mm) provided with an axial thermocouple sliding inside a tube of 1.2 mm external diameter. The catalyst particle size was 35–52 mesh obtained by grinding the granules prepared by pressing the calcined powder at 1300 kg/cm² for 5 min. The catalyst charge ranged between 4 and 5 g. The feed consisted of 6.5% C_3H_6, 13% O_2 (the balance being N_2) at 200–300 ml min^{-1} (at STP) total gas flow. A manometer was placed at the reactor inlet for measuring the

actual pressure. The reactants and products were analyzed by GC on different columns; a molecular sieve column 1.2 m long at room temperature for O_2, N_2, and CO and a Porapak QS 2-m column at 150°C for air, CO_2, H_2O, propylene, and acrolein. After reaction, the catalyst was quenched down to room temperature under nitrogen.

RESULTS AND DISCUSSION

DT, TG, and DSC Analyses

Figure 1 gives the DTA thermograms in air of FeMo-O(I), FeMoBi-0.064, and Fe MoTe-0.064 samples dried at 120°C.

FeMo-O(I) showed two exothermic peaks with maxima at T = 256°C and T = 300°C, both with shoulders, due to different nitrate decompositions and an endothermic peak at T = 344°C and a broad exothermic peak at 350–400°C due, respectively, to the evolution and combustion of ammonia.

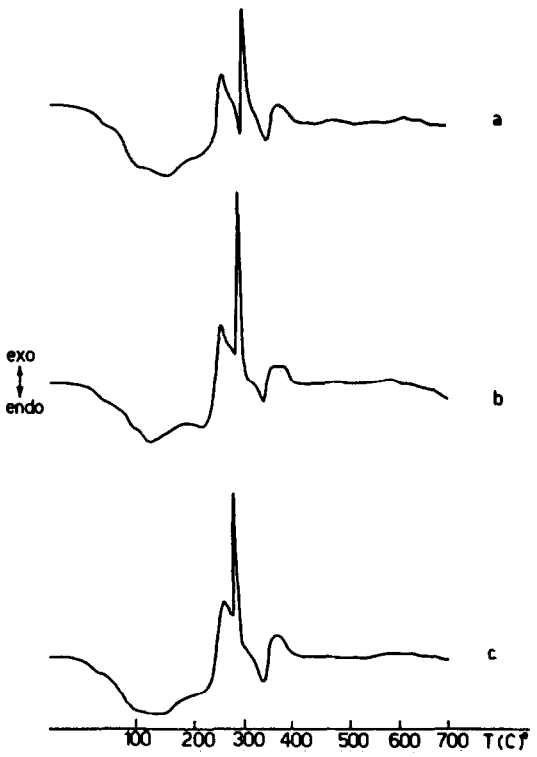

FIG. 1. DTA thermograms in air of FeMo-0(I) (a), FeMoBi-0.064 (b), and FeMoTe-0.064 (c).

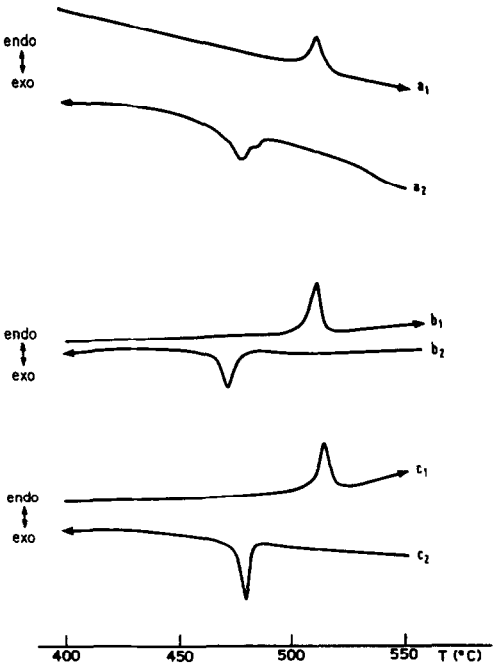

FIG. 2. DSC thermograms of FeMo-0(I) (a_1, on heating; a_2, on cooling), FeMoBi-0.256 (b_1, b_2), and Fe MoTe-0.256 (c_1, c_2).

FeMoBi-0.064 and FeMoTe-0.064 thermograms were similar to that of FeMo-0(I); slight differences concerned the nitrate decomposition and the exothermic peak associated with the oxidation of ammonia.

TG analyses of FeMo-0, FeMoBi, and FeMoTe samples calcined at 510°C did not show any weight loss up to 700°C.

DSC thermograms of FeMo-0(I), Fe MoBi-0.256, and FeMoTe-0.256 calcined at 380°C are given in Fig. 2.

All the samples showed an endothermic peak on heating at T = 513–515°C and an exothermic peak on cooling at 475–481°C, that can be attributed to the ferroelastic transition (monoclinic ⇄ orthorhombic) of $Fe_2(MoO_4)_3$ (*24*, *25*). The intensity and the shape of the peaks became reproducible after the first temperature cycle, which indicates that the catalyst samples calcined at 510°C are stable. The shape of the exothermic and endothermic peaks and the enthalpy change associated with the peaks depended on the presence of Bi and Te. These

data indicate that the $Fe_2(MoO_4)_3$ structure is modified by doping of Bi and Te.

X-Ray Data

Table 1 shows the X-ray patterns of FeMo-0(I), FeMoBi-0.256, and FeMoTe-0.256 calcined at 510°C.

The pattern of FeMo-0(I), as well as that of FeMo-0(II), is in good agreement with literature data for $Fe_2(MoO_4)_3$ (*26–30*). No appreciable amount of MoO_3 was detected in the two samples. FeMoBi-0.256 showed the presence of $Bi_3(FeO_4)$ $(MoO_4)_2$ in addition to $Fe_2(MoO_4)_3$ [peaks at d = 4.89, 4.79, 3.179 and 2.69 Å and reinforcement of peaks at d = 3.14 and 2.63 Å (*23, 31*)]. No MoO_3 peaks were observed nor bismuth molybdate phases detected. FeMoTe-0.256 showed the presence of MoO_3 in addition to $Fe_2(MoO_4)_3$ [peaks at d = 6.93, 3.81, 3.26, and 3.01 Å and reinforcement of peaks at d = 3.46 and 2.65 Å (*32*)]. Neither the ternary compound Fe(III)–Mo–Fe-0 (*17*) nor Te_2MoO_7 (*33*) was observed.

TABLE 1

X-ray Powder Diffraction Patterns

FeMo-0(I)		FeMoTe-0.256		FeMoBi-0.256	
d (Å)	I/I_0	d (Å)	I/I_0	d (Å)	I/I_0
		6.93	35		
6.39	14	6.39	16	6.39	13
5.77	28	5.765	29	5.77	30
				4.89	9
				4.79	12
4.55	14	4.55	8	4.55	13
4.33	40	4.33	37	4.33	46
4.08	58	4.08	58	4.08	60
3.90	52	3.90	46	3.91	51
3.87	100	3.87	100	3.87	100
		3.81	32		
3.74	13	3.735	17	3.74	17
3.56	25	3.56	29	3.56	28
3.464	62	3.464	111	3.464	63
3.347	10	3.347	17	3.35	12
		3.26	64		
3.24	45	3.24	61	3.245	48
3.20	15	3.195	27	3.20	21
				3.179	48
3.135	8	3.135	12	3.14	58
		3.01	4		
2.955	25	2.95	27	2.955	27
2.89	10	2.89	8	2.89	13
2.84	18	2.84	15	2.85	22
				2.69	9
2.65	11	2.65	26	2.65	13
2.63	22	2.63	29	2.63	30

The presence of $Bi_3(FeO_4)$ $(MoO_4)_2$ was detected in samples with Bi content above 0.064 and increased with Bi content while the amount of crystallized $Fe_2(MoO_4)_3$ phase decreased (see Fig. 3). The $Bi_3(FeO_4)$ $(MoO_4)_2$ X-ray peaks increased with higher calcination temperatures (600, 700, and 800°C) while those of $Fe_2(MoO_4)_3$ showed only slight increases. The greater the Bi loading, the smaller was the amount of crystallized $Fe_2(MoO_4)_3$ at 600–700°C which, however, was far below the levels in FeMo-0 at the same temperature. These results confirm that the smaller amount of crystallized $Fe_2(MoO_4)_3$ in FeMoBi catalysts at 700–800°C is due to the formation of $Bi_3(FeO_4)$ $(MoO_4)_2$ and indicate a more microcrystalline or amorphous nature of the samples at 510°C.

In FeMoTe catalyst with Te content above 0.00064, MoO_3 was detected but the quantity present did not properly follow the Te content. The amount of crystallized Fe_2 $(MoO_4)_3$ decreased with Te although not in a regular way, but it was always inversely related to the amount of MoO_3 (see Fig. 4). By increasing the calcination temperature to 600°C the amounts of both crystallized $Fe_2(MoO_4)_3$ and MoO_3 increased. At 700°C MoO_3 was completely lost from the catalyst and the amount of crystallized $Fe_2(MoO_4)_3$ further increased but never reached the level of FeMo-0 at the same temperature. No crystalline Te-containing compounds were observed at calcination temperatures of 510, 600, and 700°C. X-Ray fluorescence analyses of FeMoTe-0.256 revealed a substantial loss of tellurium (approximately 35% of total Te) on going from 600 to 700°C. These data confirm that the catalysts rich in Te and calcined at 510°C consist of crystallized $Fe_2(MoO_4)_3$ and microcrystalline or amorphous compounds. These compounds

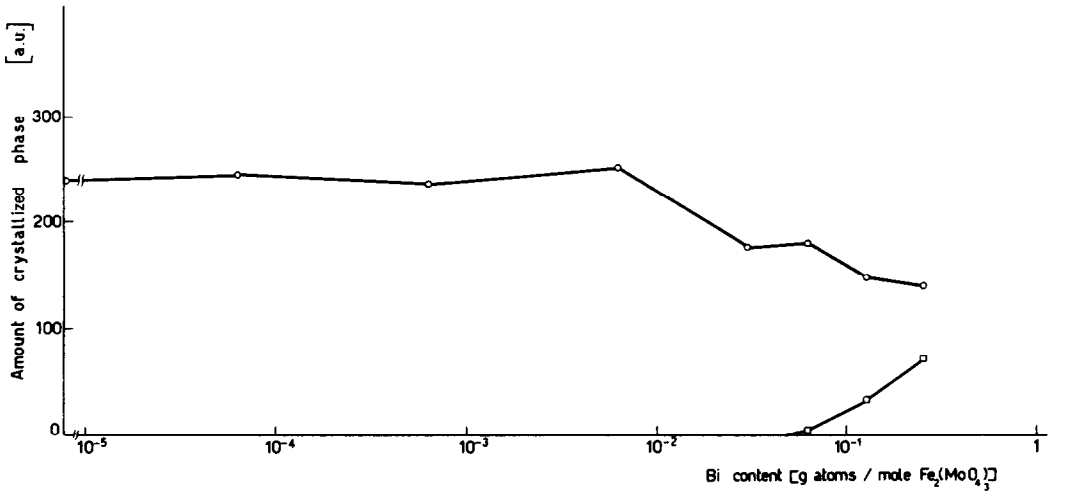

FIG. 3. Amount of crystallized phases vs Bi content in FeMoBi catalyst samples: $Fe_2(MoO_4)_3$ (○); $Bi_3(FeO_4)(MoO_4)_2$ (□). The sums of the heights of the most intense X-ray peaks of $Fe_2(MoO_4)_3$ (d = 3.24, 3.464, 3.87, 3.90, 4.08, 4.33 Å) and of $Bi_3(FeO_4)(MoO_4)_2$ (d = 4.89, 4.79, 3.179, 3.14, 2.69, 2.63 Å) were taken as a measure of the amounts of the two crystallized phases. Appropriate corrections were considered for the X-ray peaks at d = 3.14 and 2.63 Å, which are common to both $Fe_2(MoO_4)_3$ and $Bi_3(FeO_4)(MoO_4)_2$.

transform with temperature into $Fe_2(MoO_4)_3$ and MoO_3, which is lost from the catalyst together with substantial amounts of Te at higher temperature. The X-ray investigation further confirmed the absence of appreciable amounts of either crystalline phases other than $Fe_2(MoO_4)_3$ or microcrystalline and amorphous phases in catalyst samples with low content of Bi or Te.

Infrared Spectra

Figure 5 shows the infrared spectra of FeMo-0(I), FeMoBi-0.256, and FeMoTe-0.256 samples calcined at 510°C together with that of $Bi_3(FeO_4)(MoO_4)_2$ as reference. The spectrum of FeMo-0(I) is in agreement with literature data for $Fe_2(MoO_4)_3$. The very weak shoulder at 990 cm^{-1} can be as-

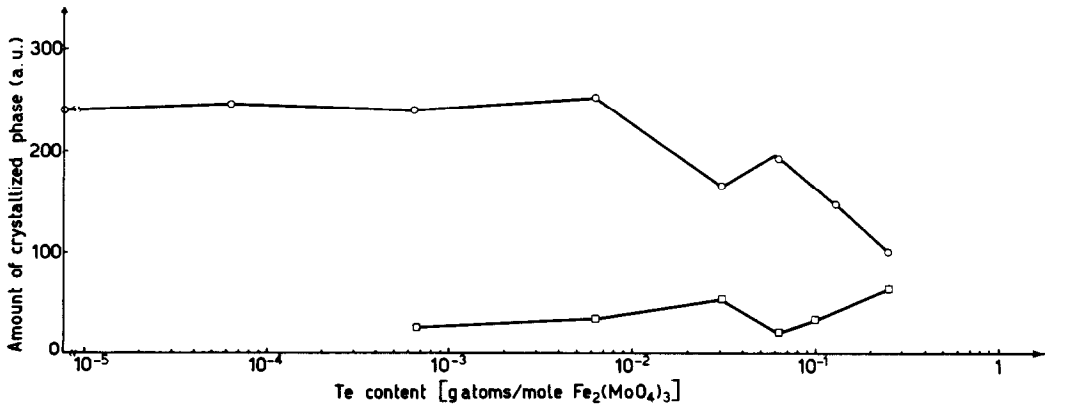

FIG. 4. Amount of crystallized phases vs Te content in FeMoTe catalyst samples: $Fe_2(MoO_4)_3$ (○); MoO_3 (□). The quantity of crystallized MoO_3 was measured from the sum of the heights of the X-ray peaks at d = 6.93, 3.81, 3.464, 3.26, and 2.65 Å. Appropriate corrections were made for the X-ray peaks at d = 3.464 and 2.65 Å which are common to both $Fe_2(MoO_4)_3$ and MoO_3.

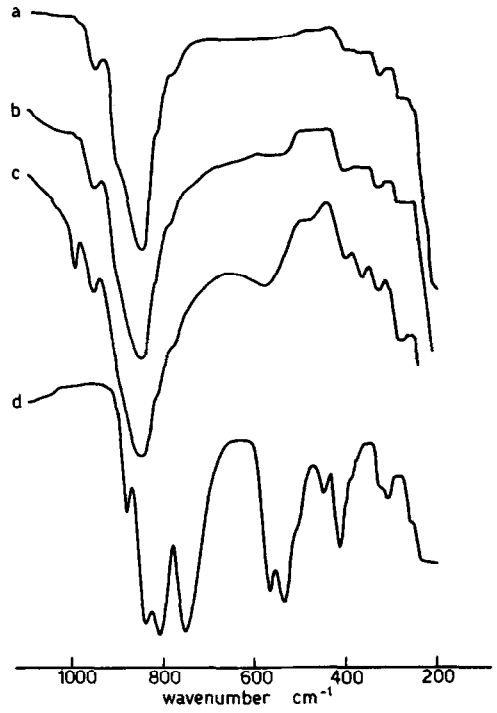

FIG. 5. Infrared spectra of: FeMo-0(I) (a); FeMoBi-0.256 (b), FeMoTe-0.256 (c), and $Bi_3(FeO_4)(MoO_4)_2$ (d).

signed to a Mo=O stretching mode, with Mo in octahedral coordination. This shoulder is slightly more intense in FeMo-0(II).

The spectrum of FeMoBi-0.256 showed additional absorption bands at 410, 530, and 750 cm^{-1} together with an enlargement of the main absorption band at 850 cm^{-1}. All these modifications are consistent with the presence of $Bi_3(FeO_4)$ $(MoO_4)_2$ (*31*), in agreement with X-ray data.

The spectrum of FeMoTe-0.256 showed absorption bands at 990, 580, and 370 cm^{-1} attributed to the MoO_3 phase and an enlargement of the band at 850 cm^{-1} which can be explained by the superposition of the main complex band of FeMo-0 at 850 cm^{-1} and the absorption band typical of MoO_3 at 860 cm^{-1}. The data are again in agreement with the X-ray results.

The typical absorptions of $Bi_3(FeO_4)$ $(MoO_4)_2$ in FeMoBi samples and of MoO_3 in FeMoTe samples were also observed, although with lower intensity, in FeMoBi-0.128 and FeMoTe-0.128, respectively.

Raman Spectra

Figure 6 shows the Raman spectra of FeMo-0(I), FeMoBi-0.256, and FeMoTe-0.256 samples calcined at 510°C together with that of $Bi_3(FeO_4)$ $(MoO_4)_2$ as reference.

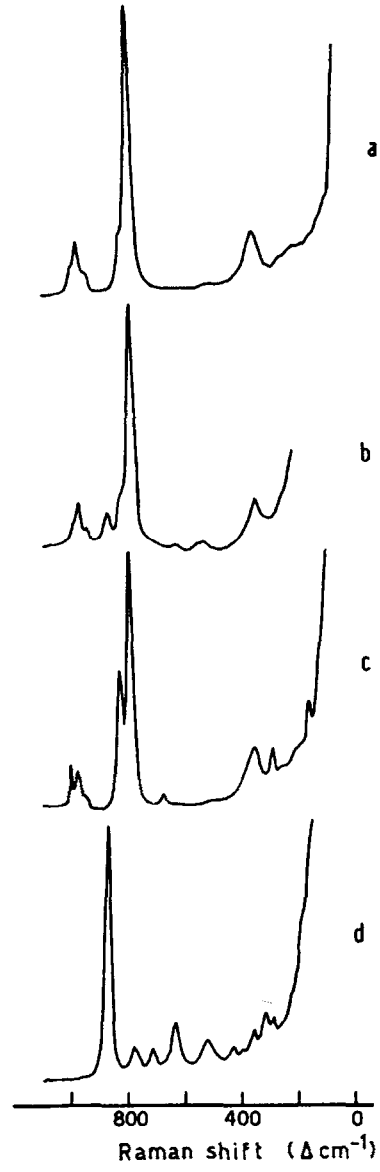

FIG. 6. Raman spectra of: FeMo-0(I) (a), FeMoBi-0.256 (b), FeMoTe-0.256 (c), and $Bi_3(FeO_4)(MoO_4)_2$ (d).

The Raman spectrum of FeMo-0(I) is in agreement with the literature data for $Fe_2(MoO_4)_3$ (*8*). The shoulders at 820 and 990 cm^{-1} are consistent with trace amounts of Mo octahedrally coordinated with oxygen. These shoulders were slightly more intense in FeMo-0(II).

FeMoBi-0.256 showed additional bands at 640 and 875 cm^{-1} which can be attributed to $Bi_3(FeO_4)(MoO_4)_2$.

FeMoTe-0.256 showed new bands at 280 and 660 cm^{-1} and a strong reinforcement of the bands at 820 and 990 cm^{-1} that can be attributed to the presence of the MoO_3 phase.

The presence of the bands typical of $Bi_3(FeO_4)(MoO_4)_2$ and MoO_3 was also detected in FeMoBi-0.128 and in FeMoTe-0.128, respectively.

Diffuse Reflectance Spectra

Figure 7 shows the electronic spectra of samples calcined at 510°C. Spectra of Bi_2O_3, $NaBiO_3$, orthorhombic TeO_2, tetragonal TeO_2, and H_6TeO_6 calcined at differ-

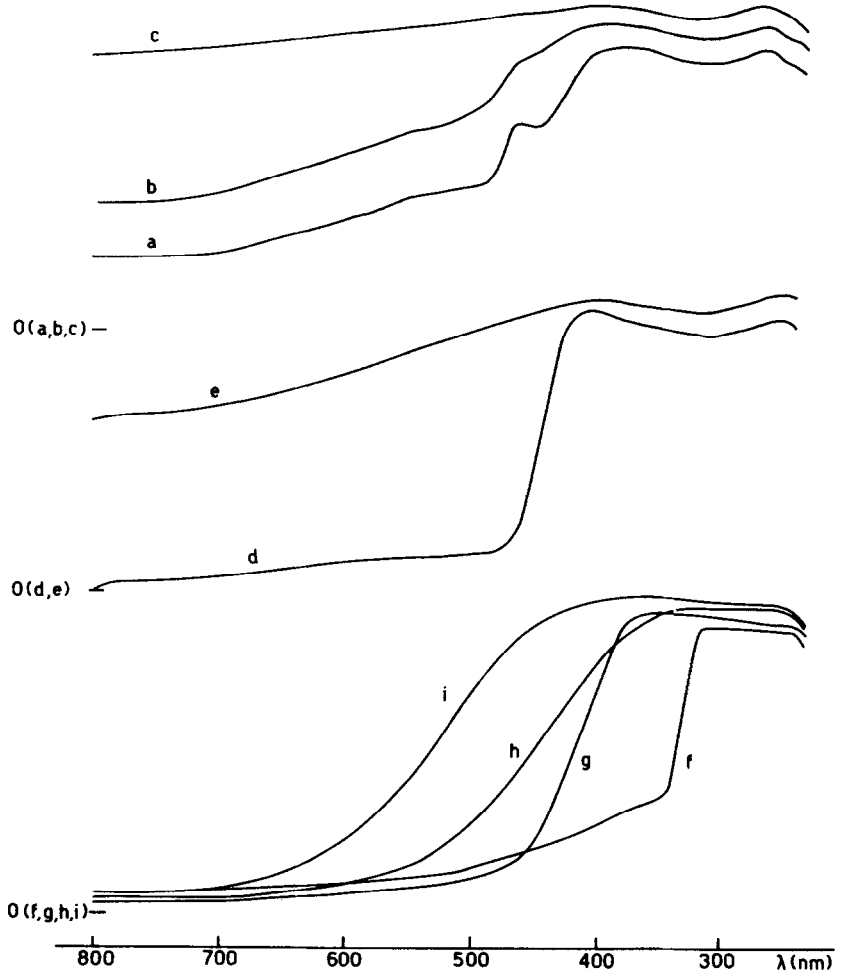

FIG. 7. Diffuse reflectance spectra of: FeMo-0(I) (a), FeMoBi-0.256 (b), FeMoTe-0.256 (c), Bi_2O_3 (d), $NaBiO_3$ (e), orthorhombic TeO_2 (f), tetragonal TeO_2 (g), H_6TeO_6 without any thermal pretreatment (h), and H_6TeO_6 calcined at 350°C for 1 hr (i).

ent temperatures are also shown for comparison.

The FeMo-0(I) spectrum exhibited an absorption edge at 400 nm due to the charge transfer process $O^{2-} \rightarrow Mo^{6+}$ (*34*) and a characteristic absorption band at about 460 nm already observed by other authors (*18, 35*). The broad absorption in the uv region indicates the presence of both tetrahedral and octahedral oxomolybdenum (VI) groups with characteristic peak maxima at 270, and at 270 and 360 nm, respectively (*36*). Mo atoms in an ideal $Fe_2(MoO_4)_3$ structure are surrounded by oxygen tetrahedrally (*29*). The absorption at 360 nm could be due to Mo(VI) accommodated in the octahedral voids available in the $Fe_2(MoO_4)_3$ structure (*30*), and/or to trace amounts of MoO_3 too small to be observed by X-ray diffraction. The absorption at 360 nm was present in both FeMo-0(I) and FeMo-0(II) catalyst samples.

FeMoBi and FeMoTe spectra showed the absorptions already present in the spectrum of FeMo-0 and an additional absorption in the visible region. This absorption was broad and increased with Bi and Te contents up to 0.032, as shown in Fig. 8 in which the absorption was measured at 500 nm. Over the 0.032 level the behavior of FeMoBi and FeMoTe catalysts differed: the absorption markedly increased with Te while it was almost constant with Bi. Appreciable departures from the general trend did occur for FeMoTe catalysts. The results clearly indicate that the absorption is associated with Bi and Te ions. Inspection of reference spectra indicates that an absorption in the visible region was also present in the case of $NaBiO_3$ and H_6TeO_6, as opposed to Bi_2O_3 and either orthorhombic or tetragonal TeO_2. The absorption in the visible region was much stronger in H_6TeO_6 calcined at 350°C, where pairs of Te^{4+} and

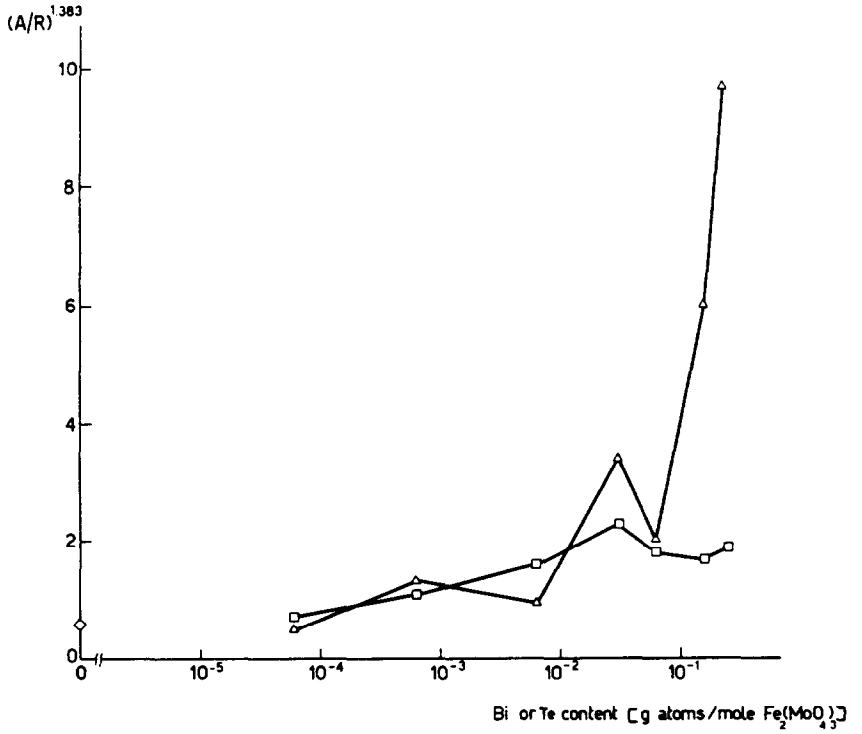

FIG. 8. Intensity of absorption at 500 nm vs Bi and Te content; $(A/R)^{1.383}$ where R = percentage reflectance and A = 100-R.

Te^{6+} are expected to be formed in larger amounts (*37*). Also, $NaBiO_3$ should be properly considered a mixed-valence compound containing small quantities of Bi^{3+} since it is difficult to prepare stoichiometric $NaBiO_3$, because of the very high oxidizing power of Bi^{5+}.

On the basis of reference spectra, the absorption of the FeMoBi and FeMoTe systems in the visible region can be assigned to electron transfer processes between nearest neighbor pairs of Bi^{5+} and Bi^{3+}, or Te^{6+} and Te^{4+}, respectively, that form oxo-bridged units. This has already been proposed for a large series of mixed-oxide systems (*38*). Selective examples in this respect are mineral crocidolite (*39*), nickel oxide (*40*), iron-doped $LiNbO_3$ (*41*), and Sb_2O_4 (*42*). All of these compounds absorb in the visible region. As already proposed in the case of mineral crocidolite, not only nearest neighbor but also longer electron jumps may be involved in the transfer process (*43*). Therefore in addition to Bi or Te, Mo and/or Fe might also be involved in the process. In any case the transfer process results in controlled valence conductivity (*38*).

The assignment of the absorption in the visible region to electron transfer processes between pairs of oxidizing and reducing ions is consistent with the constancy of the intensity of the absorption for Bi greater than 0.032 where $Bi_3(FeO_4)(MoO_4)_2$ is formed. As a matter of fact bismuth is present only as Bi^{3+} in this compound. The slight random departures from the general trend for FeMoTe samples in Fig. 8 can be explained with random amounts of oxomolybdenum (VI) groups which change the reference background absorption in the spectra.

The possibility that the absorption in the visible region is due to a new charge transfer process between Mo and/or Fe in mixed valence states such as MoO_{3-x} or Fe_3O_4, induced by the presence of Bi or Te, is unlikely for the following reasons. First, the XPS results (see Table 2) show no evidence of reduced Fe_{2p} or Mo_{3d} binding energies with Bi or Te loading, the only exception being the 0.256 Te sample. Second, the presence of Fe_3O_4 would result in a very low selectivity which was not observed. Also, the presence of MoO_{3-x} presupposes the presence of MoO_3 which was found only in the FeMoTe samples. Here, however, there was no clear correlation between the amount of MoO_3 and the visible absorption intensity (see Figs. 4 and 8).

XPS Measurements

The binding energies of the main elements present in the catalyst samples are given in Table 2 referenced to the C_{1s} contamination peak (285 eV). Data for Bi_2O_3, $NaBiO_3$, orthorhombic TeO_2, and H_6TeO_6 with no thermal pretreatment are also shown for comparison.

Although the Bi_{4f} signal would be expected to shift to higher binding energy on going from Bi_2O_3 to $NaBiO_3$ this was not the case. Apart from the problems associated with "C_{1s} referencing" for Bi compounds (*44*), the $NaBiO_3$ sample darkened during analyses, Bi probably being reduced from Bi^{5+}, giving a Bi_{4f} binding energy below that of Bi_2O_3. However, a slight increase in the Bi_{4f} binding energies was observed in Fe MoBi catalyst samples on increasing the Bi loading.

A difference of only 0.8 eV in the Te_{3d} binding energy exists between orthorhombic TeO_2 and H_6TeO_6 (Table 2 and Refs. (*45, 46*)) which makes it difficult, also in this case, to clearly identify oxidation states of Te in the different catalyst samples. However, there was a net increase in the binding energy of tellurium with increasing Te/Mo ratio at the surface (see Table 2 and Fig. 10). The Te_{3d} signals did not show any marked asymmetry differences with increases of Te loading which excludes the possibility of separate Te^{4+} and Te^{6+} species at the catalyst surface. This is consistent with the hypothesis (see diffuse reflectance spectra) of the formation of chain bonds of the type Te^{6+}–O–M–O–Te^{4+} or Te^{6+}–O–

TABLE 2

Binding Energies from XPS Results (C_{1s} = 285 eV)

Catalyst sample	Fresh (f) or used (u)	Fe_{2p}	Te_{3d}	O_{1s}	Mo_{3d}	Bi_{4f}	Fe_{3p}	Te_{4d}	Mo_{4p}
Bi_2O_3	f	—	—	530.1	—	160.0	—	—	—
$NaBiO_3$	f	—	—	530.3	—	159.5	—	—	—
Orthorhombic TeO_2	f	—	577.1	531.1	—	—	—	45.7	—
H_6TeO_6	f	—	577.9	532.0	—	—	—	46.7	—
FeMo-0(I)	f	711.5	—	530.1	233.0	—	57.9	—	42.3
FeMoBi-0.00064	f	712.5	—	531.1	233.7	—	58.7	—	43.1
FeMoBi-0.0064	f	711.9	—	530.2	232.7	160.0	57.9	—	42.3
FeMoBi-0.032	f	711.5	—	530.3	232.9	160.5	57.9	—	42.3
FeMoBi-0.032	u	711.3	—	530.2	232.8	160.1	57.5	—	41.7
FeMoBi-0.128	f	712.2	—	531.2	233.0	160.2	58.0	—	43.2
FeMoBi-0.128	u	711.7	—	530.4	233.1	160.2	57.9	—	—
FeMoBi-0.256	f	712.0	—	530.5	233.0	160.5	58.0	—	42.4
FeMoTe-0.00064	f	712.4	576.8	530.5	233.1	—	57.9	—	42.1
FeMoTe-0.0064	f	712.5	577.0	531.1	233.3	—	58.1	—	42.6
FeMoTe-0.0064	u	712.3	576.8	530.7	233.3	—	57.7	—	42.1
FeMoTe-0.032	f	713.6	578.2	532.1	234.6	—	59.1	—	43.7
FeMoTe-0.064	f	712.1	576.9	530.4	233.0	—	57.1	—	41.9
FeMoTe-0.128	f	712.4	577.3	530.7	233.2	—	57.6	—	42.0
FeMoTe-0.256	f	711.0	578.2	531.7	232.0	—	56.8	—	40.8
FeMoTe-0.256	u	712.9	577.4	531.2	233.6	—	58.0	—	42.2

Te^{4+} allowing delocalization between different tellurium oxidation states.

The formation of these Te^{6+}–Te^{4+} pairs helps to stabilize at 510°C high oxidation states of Te in the catalyst samples with high surface concentration of Te. This stabilization would not be possible without a contribution from the matrix since the oxidation state in tellurium oxides changes with temperature as follows (*37*):

$$Te^{6+} \xrightarrow{200\text{–}300^\circ C}$$

$$(Te^{4+} + Te^{6+}) \xrightarrow{400\text{–}450^\circ C} Te^{4+}.$$

Quantitative data from XPS measurements are shown in Table 3 (FeMo-0(I) and FeMo-0(II)), Fig. 9 (FeMoBi catalysts), and Fig. 10 (FeMoTe catalysts) and are given as signal intensities obtained directly from the spectrometer relative to that of the corresponding Mo_{3d} signal.

FeMo-0(II) showed a significantly higher concentration of molybdenum at the surface, as compared to FeMo-0(I).

The catalyst samples containing bismuth showed a steady increase in the Bi_{4f} signal on increasing the bismuth content from 0.00064, that can be described by the equation: $Bi_s = k \ln (Bi_{tot})$ (see Fig. 9). The continuing increase in the Bi_{4f} signal above 0.032 Bi as opposed to the constancy of the absorption at 500 nm in Fig. 8 can be explained by the fact that the XPS signal comprises both Bi^{3+} and Bi^{5+} whereas the absorption at 500 nm is due solely to

TABLE 3

Quantitative XPS Data for FeMo-0 Samples

Catalyst	Fe_{2p}/Mo_{3d} relative intensity
FeMo-0(I)	0.348
FeMo-0(II)	0.284

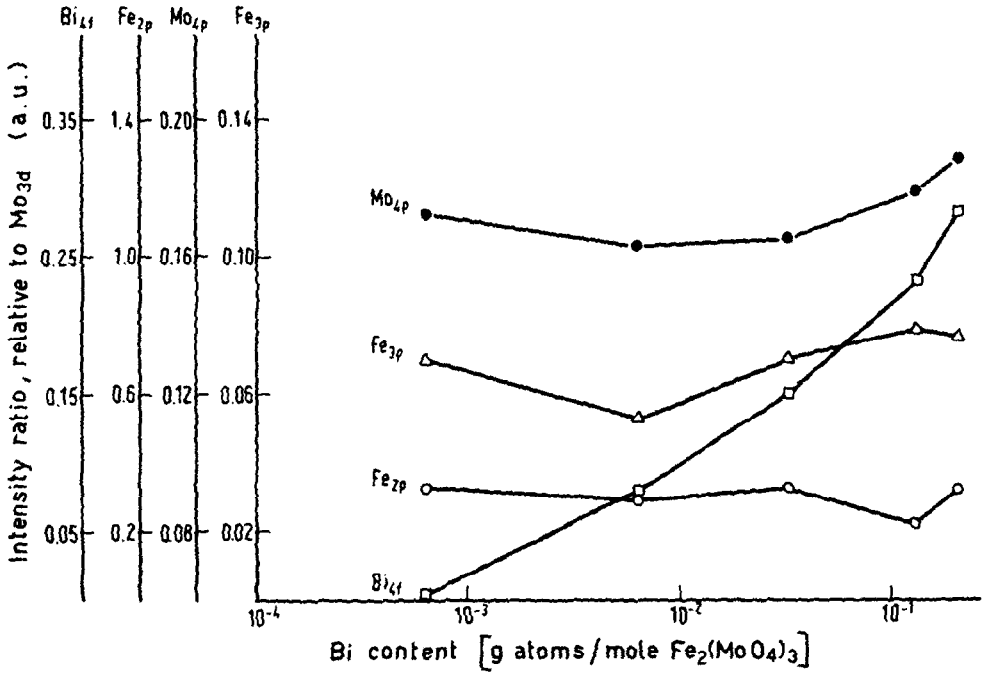

FIG. 9. Intensity ratio of XPS signals, relative to Mo_{3d}, in fresh FeMoBi catalyst samples.

Bi^{5+}–Bi^{3+} pairs, the ternary phase, $Bi_3(FeO_4)(MoO_4)_2$, formed at higher Bi loading containing only Bi^{3+}.

The Te_{3d} signal was detected in 0.00064 Te, whereas the Bi_{4f} signal was detected only with 0.0064. The Te_{3d} signal intensities from the tellurium-containing catalyst samples also increased with Te content, but in a more discontinuous manner. Up to 0.032 there was a steady increase in the Te_{3d} signal intensity ($Te_s = k \ln (Te_{tot})$, see Fig. 10), followed by a decrease at 0.064 and 0.128 Te. The most remarkable decrease from 0.064 to 0.128 Te was caused by an increase in surface molybdenum at the cost of both iron and the dopant. At the 0.256 Te level there was a sharp increase in both the Te_{3d} signal and the Fe signals to values well above their levels in 0.032 Te. Equations of the type $Me_s = k \ln (Me_{tot})$ indicate a tendency of the dopant to accumulate at the surface, the tendency being more pronounced for Te than for Bi.

The FeMoBi catalysts after use showed an oxidation state of Bi ≥ III (see Table 2), which may be attributed to a stabilizing effect of the structure. The use of the catalyst did not bring about a greater enrichment of Bi at the surface even in samples with high Bi content.

The FeMoTe catalysts after use showed an oxidation state of Te ≥ IV with both low and high Te contents (see Table 2). The surface composition was unchanged at low Te content (FeMoTe-0.0064), while at hight Te content (FeMoTe-0.256) a surface enrichment of Te, in comparison with the same sample before use, was observed, together with a partial reoxidation of Fe and Mo.

It is concluded that: (i) both catalysts with low Te and Bi content are stable with use; (ii) Te, when present in great quantity, becomes mobile and can easily be lost (see X-ray fluorescence results for FeMoTe-0.256 in the X-ray data section); (iii) catalysts with high Bi content are also stable with use.

Surface Area Measurements

In Table 4 we report the surface area of

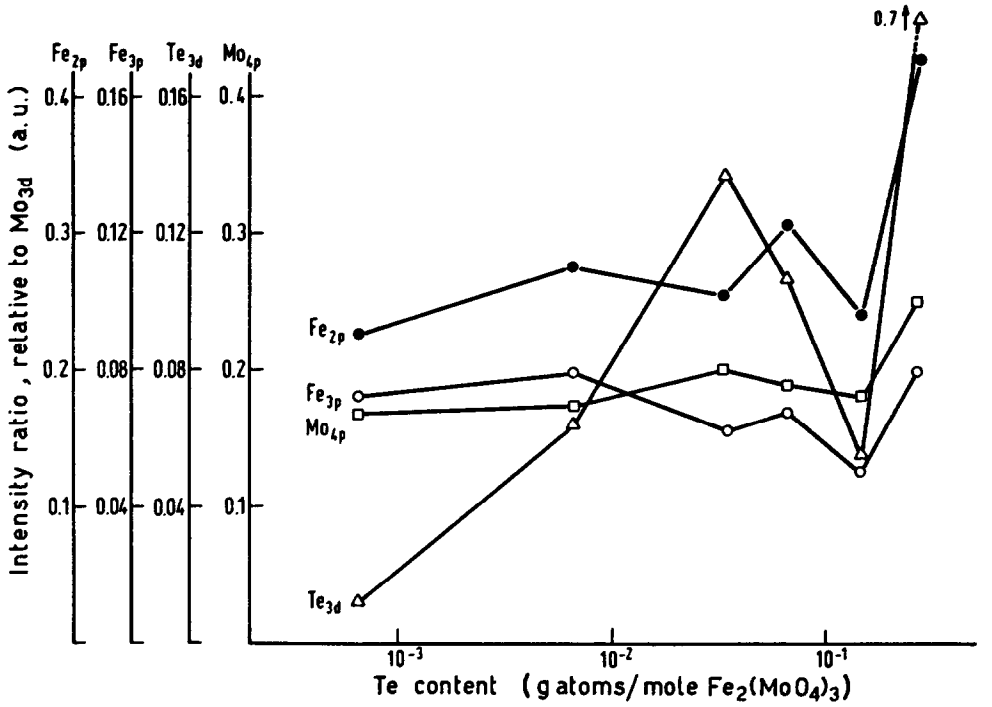

FIG. 10. Intensity ratio of XPS signals, relative to Mo_{3d}, in fresh FeMoTe catalyst samples.

the investigated catalysts before and after reaction. The surface area after reaction is generally smaller.

TABLE 4

Surface Areas of Fresh and Used Catalysts

Catalyst	Surface area before reaction (m^2/g)	Surface area after reaction (m^2/g)
FeMo-0(II)	5.5	3.9
FeMoBi-0.000064	5.4	4.0
FeMoBi-0.00064	5.4	3.9
FeMoBi-0.0064	4.1	3.5
FeMoBi-0.032	2.1	2
FeMoBi-0.064	2	1.5
FeMoBi-0.128	1.1	2.2
FeMoBi-0.252	2.2	2.5
FeMoTe-0.000064	5.4	4.1
FeMoTe-0.00064	5.4	4
FeMoTe-0.0064	5.4	3.8
FeMoTe-0.032	0.8	0.8
FeMoTe-0.064	2.2	0.8
FeMoTe-0.128	1.5	2
FeMoTe-0.256	1	0.8

Catalysts with low Bi or Te contents (below 0.032) showed surface areas comparable to those of FeMo-0, both before and after reaction. At higher Bi contents the surface areas of fresh and used catalysts were always around 2 m^2/g. Catalysts with Te contents greater than or equal to 0.032 had surface areas ranging from 2.2 to 0.8 m^2/g.

Activity Measurements

The data were analyzed by adopting a pseudohomogeneous isothermal plug flow reactor model. First-order kinetics, which is common to most MCM catalysts, for propylene consumption rate was considered:

$$r = kP_{C_3H_6}. \quad (1)$$

The assumptions of negligible radial profiles and negligible axial dispersion were based on the small reactor diameter and on L/d_p = 570—a value much larger than the critical one calculated as 30 for Pe_a = 2 and 95% conversion (*47*)—respectively. The as-

sumption of negligible temperature and concentration gradients across the film, of isothermal catalyst pellets, and of almost complete intraphase effectiveness were verified for the most severe conditions encountered in this study by computations performed along classical lines (*48*). Axial temperature profiles smaller than 5°C were measured during reaction and neglected in the analysis of the data. Computed energies of activation confirmed the negligible effect of temperature axial profiles on rate constant estimation in the present study where sizable changes in rate constant values were considered.

FeMo-0 Samples

Table 5 gives the rate constants per unit surface area (k_{sp}) and the selectivities to acrolein at 350°C for FeMo-0(I) and FeMo-0(II). Both samples show very poor selectivity while FeMo-0(II) is much more active than FeMo-0(I). Infrared, Raman, diffuse refiectance, and XPS measurements indicated that both FeMo-0 samples contained Mo octahedrally coordinated and further indicated larger amounts of octahedral Mo and a surface more enriched in Mo in FeMo-0(II). This octahedral Mo could be (i) localized in the interstitial sites of the $Fe_2(MoO_4)_3$ structure and/or (ii) present as a trace amount of MoO_3. However, MoO_3 shows very poor activity in the propylene oxidation so that it seems reasonable to relate catalyst activity for FeMo-0 samples to interstitial molybdenum, Mo_i. Actually, Mo_i can influence collective properties such as electrical conductivity and oxygen mobility that are known to affect catalyst activity. An investigation of the electrical properties and defect structure of the catalyst samples is in progress to clarify the actual mechanism of electrical conductivity and its relevance to activity. Regarding the accommodation of Mo ions within the $Fe_2(MoO_4)_3$ structure this is made possible by the openness and apparent flexibility of the matrix with cages with a diameter of about 5 Å and an open window 2.5 Å wide and with all the polyhedra that share corners only (*30*). Besides, it is worth noting that the $Fe_2(MoO_4)_3$ structure is related to a distorted $A_3B_2(SiO_4)_3$ garnet structure with the A sites unoccupied (*30*). These unoccupied sites are ordered and can form channels for the transport of Mo toward, or away from, the catalyst surface. Thus different levels of Mo_i migrating along these channels could explain the different surface Mo content in FeMo-0 samples. The transport of Mo ions could be induced either by thermal treatment and/or by the ferroelastic transition (monoclinic $\overset{513°C}{\rightleftharpoons}$ orthorhombic) of $Fe_2(MoO_4)_3$. In any case, for thermodynamic reasons (*49*) one should expect a surface more enriched in Mo in the catalyst samples with high interstitial Mo, as indeed seems to be the case.

TABLE 5

Catalytic Behavior of FeMo-0 Samples

Catalyst sample	k_{sp} at 350°C (mole/m² atm · min)	Selectivity to acrolein (%)	E_a (kcal/mole)
FeMo-0(I)	4.03×10^{-6}	5	25
FeMo-0(II)	2.35×10^{-5}	10	25

FeMoTe Samples

In Fig. 11 we report k_{sp} values and selectivity to acrolein at T = 360°C against Te content. The selectivity to acrolein increases from around 50% in the catalyst samples with low Te contents (0.000064–0.00064) to 96% in FeMoTe-0.256. The change in selectivity does not follow the Te content, FeMoTe-0.064 having a selectivity value definitely below the value recorded for 0.032, 0.128, and 0.256 Te. Selectivity presents a regular trend with Te concentration at the surface, as shown in Fig. 12. The departure of the FeMoTe-0.128 sample from such a trend is caused by the greater amount of surface molybdenum with respect to other samples. Because of this point 5 should properly be shifted more to the right of the diagram. Selectivity is

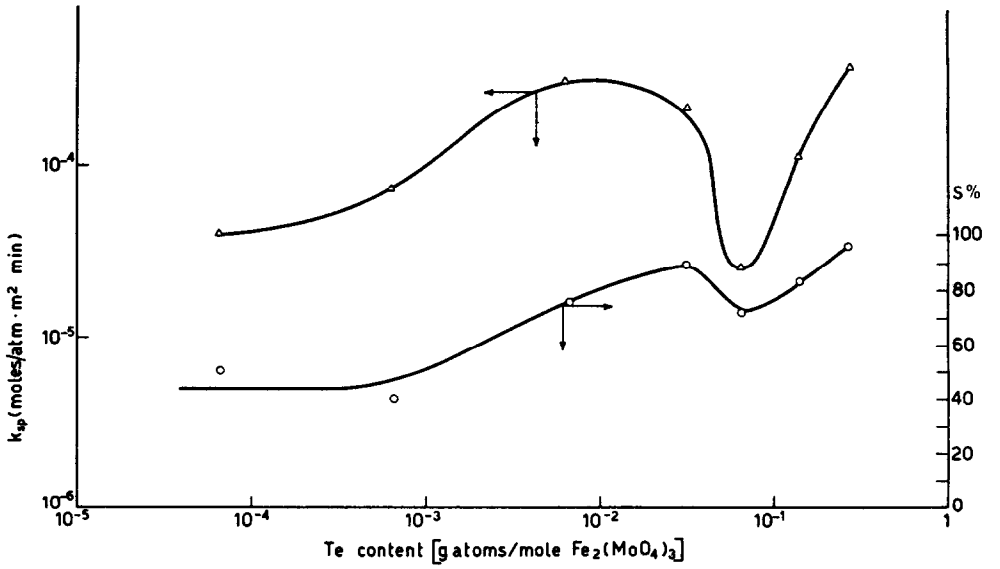

FIG. 11. Specific activity (k_{sp}) and selectivity to acrolein at 360°C vs Te content in FeMoTe catalyst samples.

also related, especially at high values, to the Te_{3d} binding energy, as shown in Fig. 13. High values of Te_{3d} binding energy imply: (i) an oxidation state of Te higher than IV; (ii) high Te/Fe or Te/Mo atomic ratio at the surface; (iii) the occurrence of chain bonds of the type Te^{6+}–O–M–O–Te^{4+} or Te^{6+}–O–Te^{4+}; (iv) controlled valence surface conductivity, characterized by two-electron transfer processes. Therefore selectivity appears to be associated with surface properties such as surface geometry and controlled surface conductivity. It is worth noting that the transfer of two electrons is also involved in the allylic mechanism of the selective oxidation of propylene.

Concerning activity, Fig. 11 showed an increase in k_{sp} from 0.000064 to 0.0064 Te, followed by a sharp decrease at 0.064. Activity is partially regained at 0.128 Te and at 0.256 Te the increase in k_{sp} is well above the level in 0.0064 Te. The anomalous behavior of k_{sp} vs Te content can be rationalized by correlating k_{sp} to the amount of MoO_3 phase

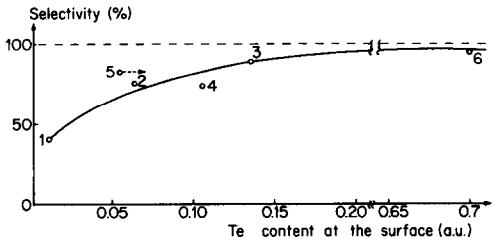

FIG. 12. Selectivity to acrolein vs Te content at the surface: (1) FeMoTe-0.00064; (2) FeMoTe-0.0064; (3) FeMoTe-0.032; (4) FeMoTe-0.064; (5) FeMoTe-0.128; (6) FeMoTe-0.256.

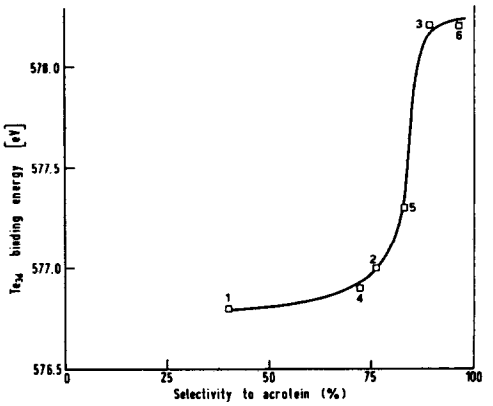

FIG. 13. Te_{3d} binding energy in fresh FeMoTe catalyst samples vs selectivity to acrolein—Numbers as in Fig. 12.

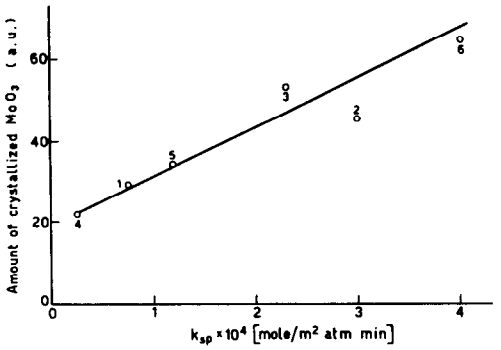

FIG. 14. Amount of crystallized MoO_3 vs specific activity (k_{sp}) in FeMoTe catalyst samples—Numbers as in Fig. 12.

that was detected by X-ray diffraction in the catalyst samples (see Fig. 14).

The presence of sizable amounts of MoO_3 in the FeMoTe catalyst samples can be explained considering that during preparation Mo is sequestrated because of the presence in the starting solution of heteropolyanions $(Te^{VI}Mo_6O_{24})^{3-} \cdot nH_2O$ (*50–52*). The presence of heteropolyanions further explains the relation observed between the amount of crystallized $Fe_2(MoO_4)_3$ and MoO_3 and the formation of amorphous TeMo compounds at high Te contents. MoO_3 is likely formed, together with the insertion of Mo in interstitial sites of the $Fe_2(MoO_4)_3$ structure, from a precursor amorphous compound. Therefore k_{sp} values should properly be related to interstitial Mo, Mo_i, and not to the amount of MoO_3 phase for reasons already discussed in the case of FeMo–0 samples.

As for the accommodation of Te it seems likely that Te ions are localized in the interstitial sites of the $Fe_2(MoO_4)_3$ structure as already proposed for Mo. Actually, this type of interstitial Te, Te_i, should reduce Fe and Mo in $Fe_2(MoO_4)_3$ assuming that the electrons are localized at metal ions on regular lattice sites. This indeed was observed from XPS binding energies in FeMoTe-0.256.

An alternative explanation involving substitution of Mo^{6+} by Te^{4+} in the lattice would lead to significant lattice deformation that was not observed. Besides, substitution of Mo^{6+} by Te^{6+} implies Te^{6+} ions tetrahedrally coordinated to oxygen which is not in line with the preference of Te^{6+} in molybdates for octahedral coordination (*53–55*).

The presence of Te_i in the lattice may also increase activity through a synergic action with Mo_i. Finally, Te_i can also migrate with the same mechanism as Mo_i in the FeMo-0 samples (see above), and even more easily than Mo_i leading to a surface enrichment of tellurium.

In Fig. 15 we report the activation energies at temperatures lower and higher than 350°C as a function of the Te content. The two values that are almost identical in FeMo-0 (E = 25 kcal/mole) tend to differentiate even at the lowest Te level: the energy of activation at $T < 350$°C is almost constant with Te, while the energy of activation at $T > 350$°C drops down to ~10 kcal/mole. It is worth noting that global isothermal inter–intraphase effectiveness is always very close to 1 either below or above 350°C so that the change with temperature of the energy of activation of FeMoTe systems indicates a change in the chemical nature of the rate-determining step of the reaction. This change is clearly brought about by the presence of Te and it is also in line with the high selectivity of the entire Fe MoTe series of catalysts (50–96%) as opposed to FeMo-0 samples. This correspondence further supports the hypothesis of associating both the changes in selectivity and energy of activation with temperature to a specific action of the dopant Te.

FeMoBi Samples

The catalytic behavior of the FeMoBi system is summarized in Figs. 16 and 17. Figure 16 gives k_{sp} and selectivity to acrolein at 360°C vs Bi content. Figure 17 gives the activation energies at T lower and higher than 350°C as a function of Bi content. Selectivity to acrolein increases from 0 to 90% with Bi content. The change in selectivity compares well with the concen-

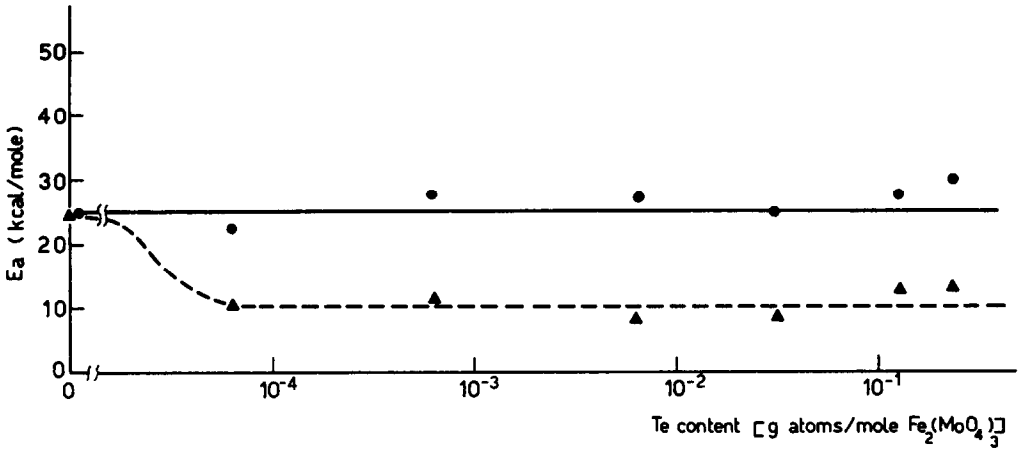

FIG. 15. Activation energies at $T < 350°C$ (●) and at $T > 350°C$ (▲) vs Te content in FeMoTe catalyst samples.

tration of Bi at the surface up to 0.032 Bi, before the formation of $Bi_3(FeO_4)(MoO_4)_2$.

A slight increase in Bi_{4f} binding energy was observed on increasing the Bi content due to the stabilizing effect of the $Fe_2(MoO_4)_3$ matrix on higher Bi oxidation states. The presence of Bi^{5+}–Bi^{3+} pairs was confirmed by the increase in the intervalence-band absorption in the visible region. These pairs of ions should accumulate at the catalyst surface because of the tendency of Bi to be concentrated at the surface. As already discussed in the case of the FeMoTe system, this type of situation would result in a well-defined surface geometry characterized by chain bonds Bi^{5+}–O–M–O–Bi^{3+} or Bi^{5+}–O–Bi^{3+} and furthermore in a controlled valence surface conductivity, characterized by two-electron transfer processes. These properties are expected to be primarily responsible for selectivity to acrolein. The possibility that a

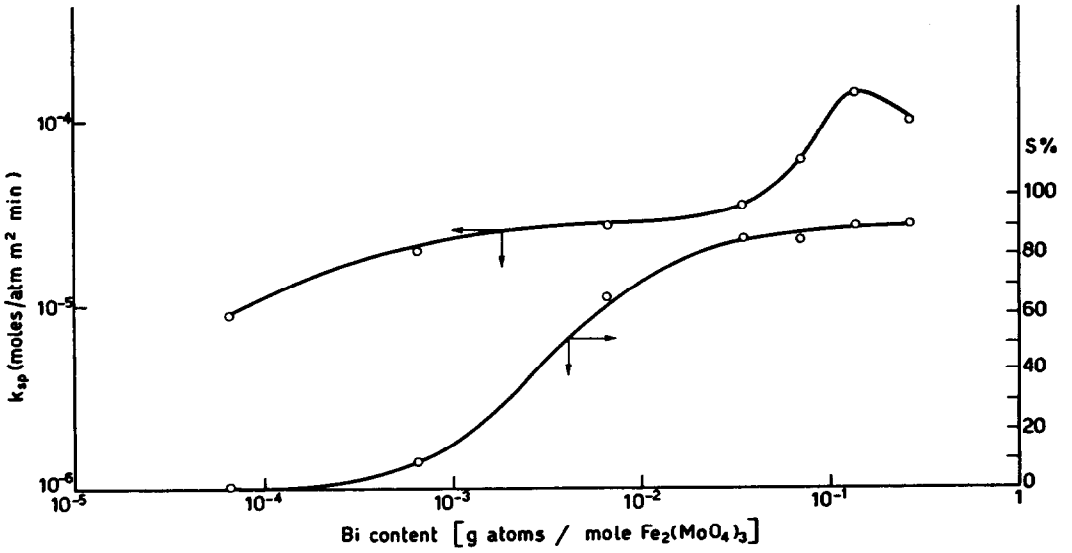

FIG. 16. Specific activity (k_{sp}) and selectivity to acrolein at 360°C vs Bi content in FeMoTe catalyst samples.

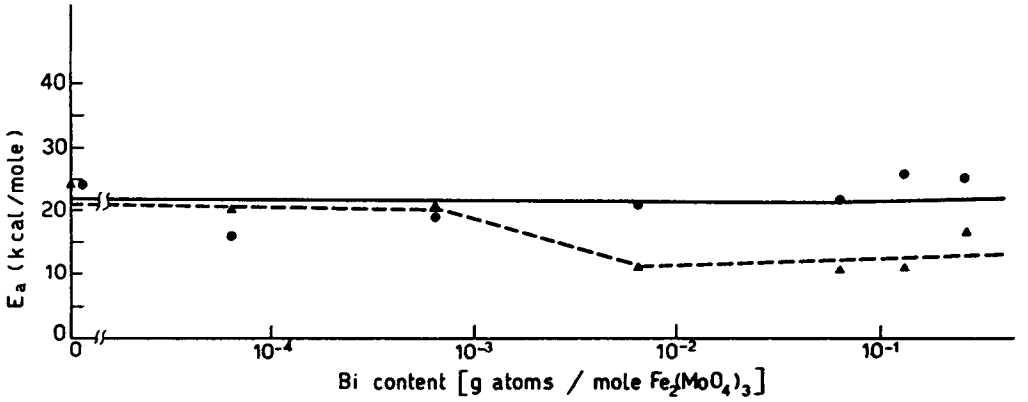

FIG. 17. Activation energies at $T < 350°C$ (●) and at $T > 350°C$ (⇵) vs Bi content in FeMoBi catalyst samples.

surface layer of the ternary phase could be responsible for the catalyst selectivity can be excluded on the basis of XPS relative intensities which show from appropriate calculations the ternary phase to be less than 5% when the selectivity has already reached 85% (FeMoTe-0.032).

k_{sp} as a function of Bi content shows a slight increase up to 0.032. The k_{sp} values in this region are practically in between the values measured for FeMo-0(I) and FeMo-)(II). A sharp increase occurs in the range 0.032–0.128 and at the 0.256 Bi level k_{sp} seems to decrease slightly. Infrared and Raman spectra of the catalyst samples with the lower Bi contents (below 0.032) showed the presence of trace amounts of octahedral Mo, while ir and X-ray data of the catalysts rich in Bi confirmed that $Bi_3(FeO_4)(MoO_4)_2$ is formed above 0.032. The amount of $Bi_3(FeO_4)(MoO_4)_2$ increased with Bi. In analogy with FeMo-0 and FeMoTe catalyst samples, the activity of FeMoBi samples up to 0.032 Bi can be associated with the presence of octahedral interstitial Mo. The sharp increase in activity over 0.032 Bi may be associated with changes in bulk properties due to the formation of the ternary-phase $Bi_3(FeO_4)(MoO_4)_2$.

The energies of activation at temperatures above and below 350°C as a function of Bi (Fig. 17) show that below 350°C it is about 20–25 kcal/mole for all catalyst samples, whereas above 350°C it decreases to ~10–15 kcal/mole on increasing the Bi content.

Also in this case the change with temperature of the energy of activation was confirmed to be associated with the change in the chemical nature of the rate-determining step. The behavior of this change against Bi content compares well with the selectivity behavior, which further supports the hypothesis of associating the two changes with a specific action of the dopant Bi.

It is worth noting that the energy maxima of the two-electron optical charge transfer transition ($Bi^{3+} \rightarrow Bi^{5+}$ and $Te^{4+} \rightarrow Te^{6+}$) in the Bi and Te reference compounds lie between 400 and 500 nm (equivalent to 18 and 14 kcal/mole for the thermal transition calculated from the Hush equation (*56*, *57*) for a symmetrical system). The diffuse reflectance spectra of the doped catalyst samples show the extension of the absorption further into the visible region, corresponding to even lower thermal transition energies.

These values are very close to the activation energy of the oxidation of propylene to acrolein above 350°C for both Bi- and Te-containing selective catalysts (10–15 kcal/mole) and this correspondence further supports the general picture put forward in this paper to explain selectivity.

Finally, the nature of the interstitial sites which can equally accommodate ions hav-

ing different coordination numbers and the flexibility of the matrix with the polyhedra sharing only corners allow interstitially located Te, Bi, or Mo to change coordination or to become coordinatively unsaturated at the surface of the catalyst thus providing sites for reactive chemisorption.

ACKNOWLEDGMENT

Two of the authors (P.F. and P.L.V.) acknowledge financial support from Italian C.N.R. (Rome).

REFERENCES

1. Sennewald, K., Gehrman, K., Vogt, W., and Shafer, S., German Offer, 1, 125, 901, to Knapsack (December 19, 1959).
2. Giochi, Y., and Shigeo, I., Japan Appl., 56, 644, to Nippon Kayaku (December 6, 1964).
3. Grasselli, R., Miller, A., and Hardman, H., U.S. Appl., 85, 722, to SOHIO (October 30, 1970).
4. Giordano, N., Gaporali, G., and Ferlazzo, N., Italian Patent, 682, 880, to Sicedison (July 14, 1961).
5. Aykan, K., Halvorson, O., Sleight, A. W., and Rogers, D. B., *J. Catal.* **35,** 401 (1975).
6. Sleight, A. W., Aykan, K., and Rogers, D. B., *J. Solid State Chem.* **13,** 231 (1975).
7. Sleight, A. W., *in* "Advanced Materials in Catalysis" (J. J. Burton and R. L. Garten, Eds.), p. 181. Academic Press, New York, 1977.
8. Villa, P. L., Szabo, A., Trifirò, F., and Carbucicchio, M., *J. Catal.* **47,** 122 (1977).
9. Andrushkevich, T. V., Boreskov, G. K., Kutzentsova, L. M., Phyasova, L. M., Tyurin, Yu.N., and Shehekochikhin, Yu.M., *Kinet. Katal.* **15,** 424 (1974).
10. Forzatti, P., Villa, P. L., Ercoli, D., Ercoli, G., Gasparini, F., and Trifirò, F., *Ind. Eng. Chem. Prod. Res. Dev.* **16,** 26 (1977).
11. Forzatti, P., and Trifirò, F., *React. Kinet. Catal. Lett.* **3,** 275 (1979).
12. Veath, F., Callahan, J. L., Idol, J. D., and Milberger, E. C., *Chem. Engl. Prog.* **5b,** 65 (1960).
13. Robin, J. Y., Arnaud, Y., Guidot, J., and Germain, J. E., *R. Acad. Sci. Ser. C* **280,** 921 (1975).
14. Linn, W. J., and Sleight, A. W., *J. Catal.* **41,** 134 (1976).
15. Forzatti, P., Trifirò, F., and Villa, P. L., *J. Catal.* **55,** 52 (1978).
16. Forzatti, P., Pasquon, I., and Trifirò, P., *in* "Proceedings of the Climax 3rd International Conference on the Chemistry and Uses of Molybdenum" (H. F. Barry and P. C. H. Mitchell, Eds.), pp. 128–131. Ann Arbor, Mich., 1979.
17. Forzatti, P., and Tittarelli, P., *J. Solid State Chem.* **33,** 421 (1980).
18. Wolf, M. W. J., and Batist, P. A., *J. Catal.* **32,** 25 (1974).
19. Matsuura, I., and Wolf, M. W. J., *J. Catal.* **37,** 174 (1975).
20. Matsuura, I., *in* "Proceedings, 7th International Congress on Catalysis, Tokyo, 1980," paper B31.
21. Prasada Rao, T. S. R., and Menon, P. G., *J. Catal.* **51,** 64 (1978).
22. Bertolini, N., Ferlazzo, N., and Ghirga, M., 1st Italian National Congress on Catalysis, Bologna, July 1979.
23. Sleight, A. W., and Jeitschko, W., *Mater. Res. Bull.* **9,** 951 (1974).
24. Sleight, A. W., and Brixner, L. H., *J. Solid State Chem.* **7,** 172 (1973).
25. Massarotti, V., Flor, G., and Marini, A., *J. Appl. Crystallogr.* **14,** 64 (1981).
26. Klevtsov, P. V., Klevtsova, R. F., Kefeli, L. M., and Plyasova, L. M., *Inorg. Mater. (USSR)* **1,** 843 (1965).
27. Plyasova, L. M., Klevtsova, R. F., Borisov, S. V., and Kefeli, L. M., *Dokl. Akad. Nauk USSR* **167,** 84 (1966).
28. Fagherazzi, G., and Pernicone, N., *J. Catal.* **16,** 321 (1970).
29. Van Truong, N., Tittarelli, P., and Villa, P. L., *in* "Proceedings of the Climax 3rd International Conference on the Chemistry and Uses of Molybdenum" (H. F. Barry and P. C. H. Mitchell, Eds.), pp. 161–165. Ann Arbor, Mich., 1979.
30. Chen, H., *Mater. Res. Bull.* **14,** 1583 (1979).
31. Sleight, A. W., Jeitschko, W., McClellan, W. R., and Weiher, J. F., *Acta Crystallogr. Sect. B* **32,** 1163 (1976).
32. Swanson, F., N. B. S., Vol. 3, Circular 539 (1953).
33. Bart, J. C. J., Petrini, G., and Giordano, N., *Z. Anorg. Allg. Chem.* **412,** 258 (1975).
34. Dickens, P. G., and Neild, D. J., *Trans. Faraday Soc.* **64,** 13 (1968).
35. Batist, P. A., Van de Moesdijk, G. C. M., Matsuura, I., and Schuit, G. C. A., *J. Catal.* **20,** 40 (1971).
36. Mitchell, P. C. H., and Trifirò, F., *J. Chem. Soc. A,* 3183 (1970).
37. Bayer, G., *Fortschr. Mineral.* **46**(I), 41 (1969).
38. Cannon, R. D., "Electron Transfer Reactions." Butterworths, London, 1980.
39. Allen, G. C., *Transition Met. Chem. (Weinheim, Ger.)* **1,** 143 (1976).
40. Allen, G. C., and Dyke, J. M., *Chem. Phys. Lett.* **37,** 391 (1976) and references therein.
41. Clark, M. G., Di Salvo, F. J., Glass, A. M., and Peterson, G. E., *J. Chem. Phys.* **56,** 6209 (1973).
42. Sala, F., and Trifirò, F., *J. Catal.* **34,** 68 (1974).
43. Littler, J. C. F., and Williams, R. J. P., *J. Chem. Soc.,* 6368 (1965).
44. Morgan, W. F., Stec, W. J., and Van Wazer, J. R., *Inorg. Chem.* **12,** 953 (1973).

45. Bahl, M. K., Watson, R. L., and Irgolic, K. J., *J. Chem. Phys.* **66,** 5526 (1977).
46. Bahl, M. K., Watson, R. L., and Irgolic, K. J., *J. Chem. Phys.* **68,** 3272 (1978).
47. Mears, D. E., *Ind. Eng. Chem. Process Des. Dev.* **10,** 541 (1971).
48. Carberry, J. J., "Chemical and Catalytic Reaction Engineering." McGraw-Hill, New York, 1976.
49. Menon, P. G., and Prasada Rao, T. S. R., *Catal. Rev. Sci. Eng.* **20,** 97 (1979).
50. Anderson, J. S., *Nature* **140,** 850 (1937).
51. Evans, H. T., *J. Amer. Chem. Soc.* **70,** 1291 (1948).
52. Kozlowski, R., *Bull. Acad. Pol. Sci.* **23,** 1029 (1975).
53. Forzatti, P., and Tieghi, G., *J. Solid State Chem.* **25,** 387 (1978).
54. Tieghi, G., and Forzatti, P., *J. Appl. Crystallogr.* **11,** 131 (1978).
55. Sloczynski, J., and Sliwa, B., *Z. Anorg. Allg. Chem.* **438,** 295 (1978).
56. Hush, N. S., *Trans. Faraday Soc.* **57,** 557 (1961).
57. Hush, N. S., *Prog. Inorg. Chem.* **8,** 391 (1961).